Minerals Engineering 156 (2020) 106494

Contents lists available at ScienceDirect

Minerals Engineering

journal homepage: www.elsevier.com/locate/mineng

A new statistically-based methodology for variability assessment of rheological parameters in mineral processing

Sebastián Contreras[a,b], Claudia Castillo[a,c,1], Álvaro Olivera-Nappa[d,b], Brian Townley[e,c], Christian F. Ihle[a,c,*]

[a] Laboratory for Rheology and Fluid Dynamics, Department of Mining Engineering, Universidad de Chile, Beauchef 850, 8370448 Santiago, Chile
[b] Centre for Biotechnology and Bioengineering (CeBiB), Universidad de Chile, Beauchef 851, 8370448 Santiago, Chile
[c] Advanced Mining Technology Center, Universidad de Chile, Tupper 2007, Santiago, Chile
[d] Department of Chemical Engineering, Biotechnology and Materials, Universidad de Chile, Beauchef 851, 8370448 Santiago, Chile
[e] Department of Geology, Universidad de Chile, Plaza Ercilla 803, 8370450 Santiago, Chile

ARTICLE INFO

Keywords:
Rheology
Tailings
Yield stress
Variability control
Statistics

ABSTRACT

If variability of input data for rheological measurements is not adequately included, their associated uncertainty and subsequent modelling can be underrated. Mineral pulp rheology determination is commonly done through triplicate tests, with such variability reported as multiples of a standard deviation, with the potential for underestimation. In the present work, a novel statistically-based methodology for the estimation of uncertainty in the rheological characterization of mineral suspensions —and other parametric models— is proposed. From the variability of the experimental measurements and the analytical propagation of errors, a set of rheological profiles are generated using Monte Carlo simulations within a variability frame. The corresponding inverse problem for curve-fitting is solved individually, resulting in distributions of fitted parameters, which were statistically-analyzed to obtain representative values for both the parameter and its true variability. The methodology proposed herein has been used to explore the applicability and limitations of the Herschel-Bulkley and Bingham models under specific experimental and data analysis protocols, where the relevance of including low-shear-rate measurement points or yield stress measurements using alternative methods is exposed. Additionally, we present a case study on the effect of the concentration of NaCl on the rheological response of synthetic tailings consisting of quartz suspensions doped with kaolinite, bentonite and kaolinite-bentonite blends, using the proposed methodology with a concentric cylinder rheometer. Results show predominantly decreasing trends in yield stress as salt concentration increases, with non-monotonical behavior and strongest variability associated to the quartz-bentonite blend.

1. Introduction

Numerous challenges are presented nowadays to the mineral processing industry, mainly induced by the compositional variability of the currently mined deposits, technological limitations, water constraints and high energy consumption (Norgate and Haque, 2010; Ihle, 2014; Calvo et al., 2016) that the present climate change scenario implies. The need to maintain a constant and ideally growing production of copper has prompted metallurgical plants to push their operational boundaries, minimizing the use of make-up water and maximizing its recovery throughout the years (Montes and Cantallopts, 2019), treating complex ores with high fine (commonly clay) content, incorporating either desalinated or direct seawater into the process (Cisternas and Gálvez, 2018; Ihle and Kracht, 2018; Herrera-León et al., 2019). In combination with the presence of clays, higher salt contents have an impact in most unit operations, including differing water–rock-mill ball chemical interaction in the grinding process (*e.g.* Cullinan et al., 1999, showing the opposite case of the impact on mill ball material), valuable mineral recovery in the flotation stage due to slime coating (Yu et al., 2017) and flocculants overconsumption in thickeners (Connelly, 2011). These issues can be seen as drivers for changes in various operational parameters and properties of the mineral suspensions, including their rheology. There is a wealth of available research on the rheology of a number of fine suspensions, including clay minerals (*e.g.* Mpofu et al.,

* Corresponding author at: Laboratory for Rheology and Fluid Dynamics, Department of Mining Engineering, Universidad de Chile, Beauchef 850, 8370448 Santiago, Chile.
E-mail address: cihle@ing.uchile.cl (C.F. Ihle).
[1] Present address: CSIRO Mineral Resources, Santiago, Chile.

https://doi.org/10.1016/j.mineng.2020.106494
Received 23 December 2019; Received in revised form 19 May 2020; Accepted 30 May 2020
Available online 27 June 2020

2003; Ndlovu et al., 2014; Cruz and Peng, 2016; Basnayaka et al., 2017; Gräfe et al., 2017), ultrafine comminution products (Vallar et al., 1999; Tangsathitkulchai, 2003; He et al., 2004; Boger, 2013; Reyes et al., 2019), and slightly coarser fine pulps such as copper concentrates and tailings (Alejo and Barrientos, 2009; Boger, 2013; Ihle et al., 2013). A relevant parameter accounting for the rheology of hyper-concentrated mineral suspensions is the so-called yield stress (τ_0). The yield stress concept defines a limit between solid-like and liquid flow behavior. Although the theoretical discussion about its existence has been a matter of debate throughout the years (Barnes and Walters, 1985; Astarita, 1990; Bonn and Denn, 2009), its use is standard in mineral processing. In particular, the yield stress is used as a design and control parameter with applications ranging from grinding, flotation, thickening, pipeline transport systems, to monitoring the physical stability of the tailings storage facilities (Sofra and Boger, 2011). Various rheology-mineralogy relationships have been described to address the effect of clays, both in real tailings (Ndlovu et al., 2013; Cruz and Peng, 2016) and synthetic tailings (Contreras et al., 2019). The economically-attractive alternative that represents using direct seawater in flotation processes (Cisternas and Gálvez, 2018) has suggested to revisit the literature on the impact of dissolved salts and pH on the yield stress and settling of pure, common clay suspensions, where differing results for τ_0, depending on whether kaolinite or bentonite are used, have been found (Van Olphen, 1964; Rand et al., 1980; Heath and Tadros, 1983; Wu and Adachi, 2016). To pursue this topic with application to mineral processing, the rheological response of quartz-clay blends in NaCl solutions is analyzed herein as a case study to test a new methodology for the statistical treatment of the laboratory data, designed to capture the variability of model-fitted rheological parameters.

It is noted that a comprehensive model to include all the aspects that describe the rheological behavior of hyper-concentrated mineral suspensions is not available at the moment. Even if very comprehensive models were available, uncertainty coming from relevant instruments (*e.g.* those related to on-line measurement of density, concentration, flow, rheology, zeta potential, mineralogy, and water characteristics), have both random error and bias. Their propagation through the various algorithms that allow their conversion from instrumental measurements of current, voltage, conductivity, among others, to the physical magnitudes of interest can scale-up to levels that defy the potential to make accurate estimations. An example of the concurrent impact of a 15% relative uncertainty in viscosity (strongly inherited from uncertainties in concentration measurement) and a 5% relative error in volume flow can propagate to about 10% uncertainty in pipeline friction losses (Ihle and Tamburrino, 2012b). This relatively tight bound of the viscosity error measurement can be significantly higher in a reduced-water slurry scenario, where near the maximum packing limit, modest uncertainties in concentration measurement (*e.g.*, $\lessapprox$5% due to fluctuations of the specific gravity of solids in the case of online measurement) may propagate to viscosity in excess of 50% for concentrations above 90% of the maximum packing values (see, *e.g.*, Ovarlez et al., 2006, for the case of monodisperse suspensions of spheres). Therefore, there is a need to provide reasonable error estimations in rheology measurements, especially in the present, widespread demand of reduced water use that has motivated the design and operation of high-density tailing systems, where rheological parameters are most sensitive to input variables. In the present work, we deal with uncertainty in the absence of process memory, *i.e.*, oblivious of upstream bias by process-induced blending (Abichequer et al., 2011). Although rheology determination is indeed directly affected by the sampling protocol, it is assumed herein that such sampling is unbiased.

Even though efforts have been made to standardize laboratory tests, including those pertaining to rheology measurement, their results are still not always reproducible. They have shown to depend heavily on subtle details of the particular pre-treatment and post-processing protocols of each laboratory and the natural variability of the material, even in moderately controlled conditions. An eloquent example of differing results of rheology measurements even when sharing materials, measurement geometries, and protocols have been reported by Nguyen et al. (2006), with τ_0 values differing by up to 100% (see also Knight et al., 2017, for a similar study using the vane geometry). To the best knowledge of the authors, there is no similar study focused on the implications of experimental variability on rheological parameter fitting.

In this paper, we present a novel methodology for the estimation of uncertainty in the rheological characterization of a concentrated mineral pulp, which may be easily extended to any other parametric model fitted to experimental data. We apply the present method to study the effect of the concentration of NaCl on the rheological response of synthetic tailings with high kaolinite-bentonite content to complement measurements of mineral suspensions that are focused on the impact of the concentration (*e.g.* Avramidis and Turian, 1991; Alejo and Barrientos, 2009; Boger, 2013), particle size or distribution (Tangsathitkulchai and Austin, 1988; Shi and Napier-Munn, 1996; Tangsathitkulchai, 2003) or salt content (*e.g.* Reyes et al., 2019).

2. Rheology modeling

Hyper-concentrated mineral pulps, understood as an equivalent homogeneous fluid, are generally categorized as non-Newtonian fluids (Boger, 2009), *i.e.*, their rheological response (shear stress τ and apparent viscosity η_a) is coupled with the flow conditions $\dot{\gamma}$:

$$\tau = f(\dot{\gamma}), \quad \eta_a(\dot{\gamma}) = \frac{\tau}{\dot{\gamma}}. \tag{1}$$

The f function of (1) represents a generalized, time-independent rheological model. The most commonly used time-independent models to determine slurry transport properties in mineral processing are the Bingham and Herschel-Bulkley models (Barnes et al., 1989; Cruz and Peng, 2016), which have in common the incorporation of a yield stress τ_0, whose values are obtained indirectly from extrapolation of the flow curve, thus being model-dependent (a schematic view of the impact of extrapolation is depicted in Reyes et al., 2019). In the case of the Bingham model,

$$\mu_B \dot{\gamma} = \begin{cases} 0 & \text{if } \tau \leqslant \tau_0^B \\ \tau - \tau_0^B & \text{if } \tau > \tau_0. \end{cases} \tag{2}$$

Here τ_0^B is the Bingham yield stress (*i.e.* the value of the intercept of the straight line and the τ-axis), and μ_B is the Bingham viscosity. In the case of the Herschel-Bulkley model,

$$K\dot{\gamma}^n = \begin{cases} 0 & \text{if } \tau \leqslant \tau_0^{HB} \\ \tau - \tau_0^{HB} & \text{if } \tau > \tau_0^{HB}, \end{cases} \tag{3}$$

where K is the consistency coefficient and n is the flow index. These models can be used provided they can reasonably describe mineral suspensions as non-segregating, equivalent fluids, within a certain time scale (Ihle et al., 2013). Other approaches (*e.g.* stress relaxation and the vane method) give a more direct reading (Nguyen and Boger, 1983), but do not report viscosity as a result from the same test. Resulting values of the yield stress from these direct measurements tend to be consistently lower than those using indirect (extrapolation) methods (Nguyen et al., 2006), an aspect that can be interpreted as a source of bias of the method itself. Nonetheless, the use of extrapolation to obtain the yield stress is common, probably because of its simple parameter-fitting nature, with the additional benefit of obtaining a rapid estimation of K and n (or μ_B when $n = 1$) from a single run. Additionally, from a system designer's perspective, this approach gives conservative values of τ_0^{HB} (or τ_0^B), which is commonly a desirable outcome.

As is in the case of viscosity (Stickel and Powell, 2005), the yield stress has a strong dependence on particle concentration. Heymann et al. (2002) proposed an empirical relationship for the dependence of τ_0 on the volumetric concentration of solids, ϕ (an excellent review can

be found in Mueller et al., 2010, for the case of infinite Péclét number suspensions). This relationship reads:

$$\tau_0 = \tau_0^* \left[\left(1 - \frac{\phi}{\phi_m} \right)^{-2} - 1 \right], \tag{4}$$

where both τ_0^* and ϕ_m are fitting parameters, representing respectively a reference for the yield stress and the maximum packing volume fraction of the suspension. This model has been derived by analogy with the suspension viscosity models proposed by Krieger (1972) and Quemada (1977). The latter have been useful to predict viscosities at mid to high suspension concentrations both in monodisperse (Ovarlez et al., 2006; Mueller et al., 2010) and polydisperse systems (*e.g.*, Appendix data in Ihle, 2013, for concentrate viscosity measurements). This empirical concept, which defines a fluid–solid transition at a given singular solid concentration ϕ_m has been used to describe the particle concentration dependency of the yield stress of mineral suspensions. Examples are Avramidis and Turian (1991), in the case of nickel laterite, and Alejo and Barrientos (2009), both for quartz and real copper tailings. The limiting concentration ϕ_m is strongly shape-dependent (Barnes et al., 1989; Mueller et al., 2010).

3. Experimental methods and materials

3.1. Materials

3.1.1. Raw materials

For the preparation of synthetic tailings, blends of quartz and clay minerals were used. These blends consisted of a mixture of analytical quality quartz sand, kaolin clay, and montmorillonite-rich Na-bentonite. Details of these certified products, obtained and characterized by local suppliers, are presented as follows. The quartz sand was ground in a laboratory ball mill, in order to replicate the original particle size distribution of the process and to fit the requirements of the measurement equipment, 100% under 105μm (mesh #140), resulting in a P_{50} of 33.3μm. Itscertified composition is 97% SiO_2, 0.8% alumina, 0.9% feldspar, traces of mica and magnetite (<0.005%). In deionized water (pH 5.5), suspensions of this material reach an equilibrium pH *ca.* 7. The certified kaolin, as detailed by the XRD analysis performed by its provider, indicates a composition of 93.5% kaolinite and 6.5% quartz. Its particle size distribution was characterized by a P_{50} of 12.9 μm. In deionized water (pH 5.5), suspensions of this material reach an equilibrium pH 5. The montmorillonite-rich Na-bentonite used for this study, as certified by provider, has a 74% montmorillonite content, the chemical composition of this material being 62.8% SiO_2, 14.2% alumina, 3.5% Fe_2O_3, 2.8% Na_2O, 1.6% MgO, 1.4% CaO, 0.3% K_2O traces of MnO. Its particle size distribution was characterized by a P_{50} of 9.1 μm. In deionized water of pH 5.5, suspensions of this material reach an equilibrium pH 8. The particle size distributions of the raw materials (Fig. 1) were obtained by laser diffraction using a Mastersizer 2000 (Malvern Instruments), and following the instructions given by the manufacturer for the characterization of clays.

Table 1
Fine fraction composition of the 20% by weight of the total solid content of the tailing. For instance, MQ (second row) has 50% of Na-bentonite (*i.e.*, overall 10% of the solids) and 50% of fine quartz (overall 10% of the solids).

Nomenclature	Fine fraction composition **F**	Properties
MM	100% **M**	Clayey
MQ	50% **M**, 50% **Q**	Semi Clayey
KK	100% **K**	Clayey
KQ	50% **K**, 50% **Q**	Semi Clayey
MK	50% **K**, 50% **M**	Clayey
SF	–	Silica control

3.1.2. Synthetic tailings

The composition of the synthetic tailings considered herein is as follows: 80% of their mass consisted of quartz sand ground under mesh #140 (105μm), and the remaining 20% had a variable composition of fine materials (**F**) under mesh #200 (74μm). The mineral species forming the fine fraction **F** could be Na-bentonite (**M**), kaolin clay (**K**) or fine silica sand (**Q**), according to the combination:

$$\mathbf{F} = \lambda_i \mathbf{K} + (1 - \lambda_i)\mathbf{Q}, \tag{5}$$

where λ_i is the mass fraction of the clay (either **K** or **M**) relative to the total fine fraction added. Considering λ_i values of 0.5 and 1.0, the resulting synthetic tailings, their nomenclature, fine fraction composition **F** and properties are described in Table 1.

3.2. Salinity of the liquid phase

Analytical grade NaCl was used to assess the effect of salinity on tailing rheology, and its concentration in the bulk fluid was referred to as a percentage relative to seawater, according to (6):

$$\lambda_{\mathrm{NaCl}} = \frac{[\mathrm{NaCl}]_{\mathrm{suspension}}}{[\mathrm{NaCl}]_{\mathrm{seawater}}}. \tag{6}$$

The value $[\mathrm{NaCl}]_{\mathrm{seawater}} = 29.5$ g/L has been considered as a reference (Cisternas and Moreno, 2014). Therefore, salinities of 50%, 100% and 150% correspond to molar concentrations of 0.25M, 0.50M and 0.76M, respectively.

3.3. Methods

3.3.1. Rheological characterization

The rheological tests were carried out using an Anton Paar RheolabQC concentric cylinder rheometer, with measuring gap $R_o - R_i = 1.497$ mm, with $R_o = 21.00$ mm and $R_i = 19.50$ mm the outer and inner cylinder radius, respectively (CC39S cup and bob system).

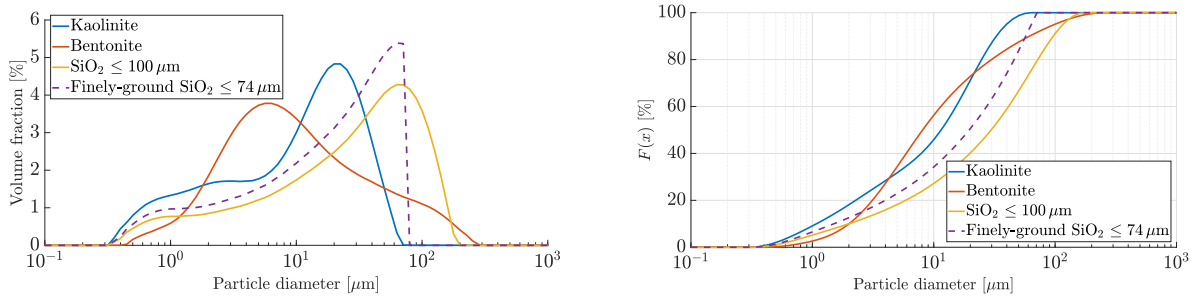

(a) Particle size distribution

(b) Cumulative particle size distribution.

Fig. 1. Particle size distribution of the raw materials used on this study. The dashed curve corresponds to the extrapolation of the fine fraction **Q**, SiO_2 under 74μm (mesh #200).

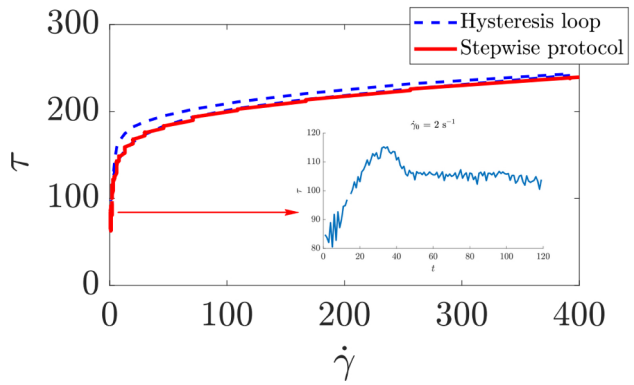

Fig. 2. Rheology measurement schematic showing the step-wise increase the shear rate.

Torque-to-stress and rotational speed-to-shear rate calculations were done following the ISO 3219 standard:

$$\dot{\gamma}_{rep} = \omega \cdot \frac{1+\delta^2}{\delta^2 - 1}; \qquad \delta = \frac{R_o}{R_i} \leqslant 1.2 \tag{7}$$

$$\tau_{\text{rep}} = \frac{1+\delta^2}{2000 \cdot \delta^2} \cdot \frac{T}{2\pi L R_i^2 C_L}. \tag{8}$$

Here, ω is the angular speed of the inner cylinder, T is the measured torque, $L = 59.83$ mm is the height of the inner cylinder (excluding the bottom cone), and C_L an end effect correction factor, assumed herein as 1.1 (as recommended by the supplier).

3.3.2. Experimental protocol

To assess the temporal behavior of the suspension and evaluate whether it exhibits thixotropy, and as standardized pre-shearing of the sample, a hysteresis test has been implemented, with shear rates increasing–decreasing linearly from 1 to 400 s^{-1} in 120 s each segment. In general, only a slight change between ascending and descending ramps has been found. This is depicted in Fig. 2. As the hysteresis loop implied considerable angular acceleration, we expect the inertia of the fluid to affect the measurements and instead use it as a pre-shearing step prior to measurement. To ensure that shear stress measurements are stable, and not the result of a transient response, flow curves have been obtained as the result of an ensemble of predefined, constant shear rates, thus mimicking a quasi-static process. The time lapse of each constant shear rate has been chosen in a logarithmic fashion (Table A.5 in Appendix A), so that there is enough time for flow stabilization at increasingly higher shear rates. Thus, for each constant value, the equilibrium shear rate response is recorded, as shown in the inset of Fig. 2 and taken as the value associated to such shear rate range. This procedure is somewhat equivalent to measuring a limited number of shear rate points, as would be required in the absence of a programmable rheometer. A further discussion regarding the data processing procedure of such experimental curves is presented in the following sections.

4. Statistically-driven methodology for assessing rheological parameters

4.1. Overview

The present methodology has three main steps, which are described below. A flow diagram is depicted in Fig. 3.

Study of error sources and choice of rheological model. First, a thorough study of the error sources associated with the experimental procedure (equipment, techniques, and protocols) must be carried out. Once their impact on the results has been estimated, it is possible to proceed with the next phase. The various error sources that should be addressed in the particular case of the present synthetic tailing rheology measurement and their phenomenological background are discussed in Section 4.2.

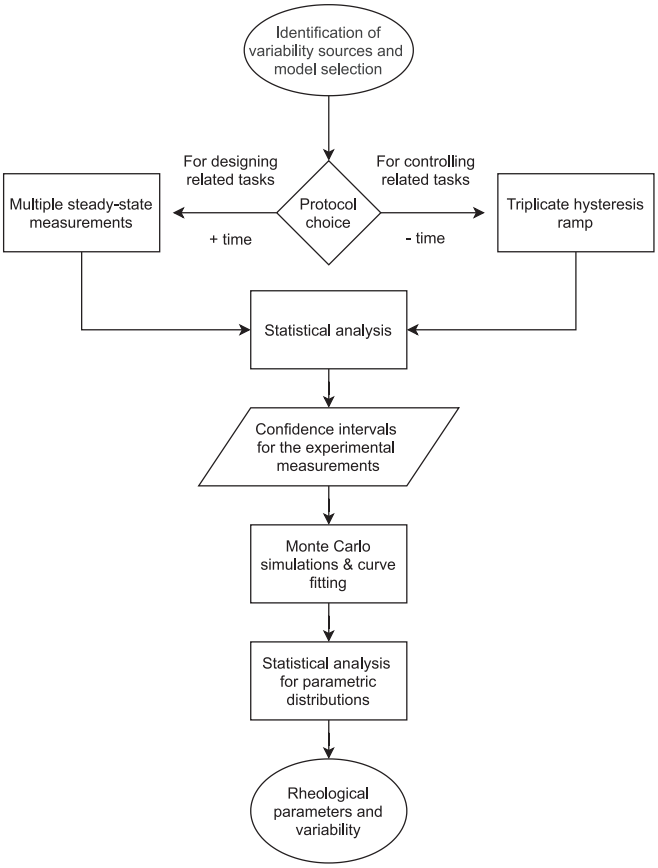

Fig. 3. Flowchart of the method proposed in this study. Stage 1: Identification of uncertainty sources both in the measurement and the suspension. *e.g.*, C_p, T, zeta potential, particle size distribution, water chemistry, among others. Selection of the rheological model. Stage 2: Selection of the experimental planning, mainly based on the time availability, the aimed confidence level and the objective of the study. Stage 3: Analysis of the experimental measurements to estimate the variability frame. Stage 4: Statistical determination of the exact confidence intervals of the measurements. Its treatment depends on the nature of the measurement. Stage 5: Simulation of N different profiles within the variability frame estimated in the previous point, which parameters would be estimated via a curve-fitting algorithm. Stage 6: Statistical determination of the exact confidence intervals of the model-derived rheological parameters obtained through the Monte Carlo simulation.

Variability estimation of experimental measurement trends, using classical statistical tools, such as the t^* multiplicative factors for the construction of confidence intervals, and variance analysis. Here we will discuss how to estimate the confidence intervals for the experimental outcome of steady-state tests, understood as the measurement of shear stress over time at a given shear rate (Section 4.3.1), and triplicate of rheological ramps (Section 4.3.2). In particular, when programming a shear rate ramp, $\dot{\gamma}(t)$, new values of $\dot{\gamma}$ do not directly transfer to constant values of the shear stress. It is required to identify the time scale for quasi static suspension equilibrium. After the variability of the experimental measurements is correctly estimated, we may set the inverse problem for curve-fitting.

Variability estimation of model-derived rheological parameters, using a Monte Carlo-inspired approach, consisting of the simulation of a set of N 'experimental' profiles within the estimated variability of the data in the previous step. After performing an

individual curve-fitting for each simulated profile, distributions of rheological parameters are obtained. Representative values of the rheological parameters and their variability are statistically obtained from such distributions.

We hereby quantify variability of a set $\boldsymbol{x}$ in terms of the coefficient of variation and the relative difference between expected measured values and real ones (also named to herein as *control* values) as:

$$CV(\boldsymbol{x}) = \frac{\sqrt{\mathrm{Var}(\boldsymbol{x})}}{\mathbb{E}(\boldsymbol{x})}, \tag{9}$$

$$e_{\mathrm{rel}} = \frac{|\mathbb{E}(\boldsymbol{x}) - x^{\mathrm{control}}|}{x^{\mathrm{control}}}. \tag{10}$$

4.2. Identification of error sources

4.2.1. Error propagation for the volumetric concentration ϕ

It is well-established that among the most influential variables on the rheology of suspensions is the particle concentration, ϕ (Mueller et al., 2010). In mineral processing plants, the solids concentration by weight, C_p, is rather used. It is straightforward to show that its relationship with ϕ is given by the following expression:

$$\phi = \frac{\rho_l C_p}{\rho_l C_p + \rho_s(1 - C_p)}. \tag{11}$$

On the other hand, the determination of concentration might, of course, include errors. The latter depends mostly on the measurement method used for particle concentration. In particular, whereas mass balance techniques are very robust and have little error, reliance on online measurement techniques such as densitometers, although having the advantage of providing real-time information, might add further uncertainty to measurements. The effect mentioned above might appear due to both limiting hardware conditions and, on the other hand, their common reliance on an input value of the solid specific gravity, which is indeed prone to fluctuations inherited by the variability of geological units. In the absence of salt fluctuations in the liquid phase, and assuming small temperature variations that may otherwise significantly propagate to the water-clay system rheology (Lin et al., 2016), variability may be represented by a vector $\boldsymbol{\sigma} = (\Delta\rho_s, \Delta C_p)^T$, with the sign Δ the amplitude of uncertainty around a reference values. The error propagation for ϕ can be obtained using a second-order Taylor expansion around the mean concentration $\bar{\phi}$:

$$\phi = \bar{\phi} + \nabla\phi\cdot\boldsymbol{\sigma} + \frac{1}{2}\boldsymbol{\sigma}^T H_\phi \boldsymbol{\sigma}, \tag{12}$$

where $\nabla\phi$ and H_ϕ represent the gradient and the Hessian matrix of ϕ, whose analytical components are detailed in Table B.6, Appendix B.1. A sensitivity analysis of the error in ϕ due to changes in ρ_s and C_p was carried out, showing that the latter impacts more severely on its value, especially at high concentrations (Fig. B.13, Appendix B.2).

4.2.2. Swelling clays

Swelling clays such as montmorillonite may structurally trap water molecules that would form part of the solid fraction after the sample is dried. When studying suspensions prepared in a closed system, special attention must be paid to analyze the solids concentration C_p. Differences in the C_p values calculated by mass balance and experimentally obtained from the oven might occur, and, in the case of swelling clays, may be explained by such structural entrapment of water. The apparent mass of solid (m_s^*) already includes the mass of trapped water (m_l^a), which must be subtracted from the mass of water forming the liquid phase m_l^*,

$$m_s^* = m_s + m_l^a; \qquad m_l^* = m_l - m_l^a. \tag{13}$$

An expression for the $C_p^* = C_p(m_s^*, m_l^*)$, which is the C_p value resulting from the aforementioned water entrapment is given by (14),

$$C_p^* = \frac{m_s + m_l^a}{m_s + m_l^a + m_l - m_l^a} \tag{14}$$

$$= \frac{m_s}{m_s + m_l} + \frac{m_l^a}{m_s + m_l} \tag{15}$$

$$= C_p^0 + \frac{m_l^a}{m_s + m_l}, \tag{16}$$

where $C_p^0 = C_p(m_s, m_l)$ corresponds to the value of C_p derived from a mass balance. Eq. (14) may be rewritten to obtain an explicit expression for ΔC_p, which is given by (17):

$$C_p^* - C_p^0 = \frac{m_l^a}{m_s + m_l}. \tag{17}$$

To estimate the amount of water structurally trapped in the clay, we follow the simple model proposed by Mering (1946) for the case of the bentonite:

$$m_l^a = R_{\max} C_p^{\mathrm{clay}} \eta m_s, \tag{18}$$

where $R_{\max}$ is the theoretical maximum water trapping potential of the clay, expressed in grams of water per gram of clay, C_p^{clay} the clay content of the suspension, η is a trapping efficiency, and m_s the solid mass. Hence, we can deduce a non-dimensional expression for the relative error, given by (19) as:

$$e_{\mathrm{rel}} = R_{\max} C_p^{\mathrm{clay}} \eta. \tag{19}$$

For Na-montmorillonite, $R_{\max}$ values of roughly 0.4 grams of water per gram of clay have been reported (Mering, 1946), and a trapping efficiency (η) ranging between 15% and 95%, depending on the weathering of the clay and the available hydroxyl groups in its structure. To highlight the impact that ignoring this error source would have on the ϕ values, a parametric swipe over the efficiency η has been made, showing that the relative error could be as large as 10% when working at high concentrations (see Fig. 4).

4.2.3. Measurement equipment limitations

The empirical constant C_L in (8), used in the context of the ISO 3219 standard, has recommended values ranging from 1.10 to 1.28 for non-Newtonian pseudoplastic fluids at low shear rates (provided by the manufacturer in the technical information of the rheometer). To evaluate the impact of the uncertainty in C_L on the reported shear stress values τ_{rep}, a first-order expansion yields:

$$\tau_{\mathrm{rep}} = \frac{A}{C_L}, \qquad \tau_{\mathrm{rep}}^* \approx \tau_{\mathrm{rep}} - \frac{A}{C_L^2}\Delta C_L, \tag{20}$$

where A summarizes all the multiplicative constants of (8), and τ_{rep}^* is the value of τ_{rep} after correcting C_L. It is possible to rearrange (20) to derive an expression for the relative error, given by (21):

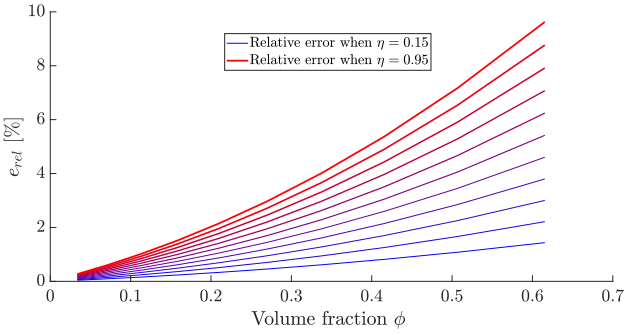

Fig. 4. Propagation of the error due to water entrapment in Na-montmorrillonite, for various different values of $R_{\max}$, as defined in (19).

$$\tau^*_{\text{rep}} - \tau_{\text{rep}} = -\tau_{\text{rep}}\frac{\Delta C_L}{C_L}, \qquad \Leftrightarrow \qquad \frac{\Delta\tau_{\text{rep}}}{\tau_{\text{rep}}} = -\frac{\Delta C_L}{C_L}. \tag{21}$$

It is therefore concluded from (21) that an uncertainty in ΔC_L of 0.1 propagates to a relative error of up to 9% in τ_{rep}.

4.2.4. Taylor-Couette instability

The flow of a fluid induced by the rotation of the inner (and/or outer) cylinder in a Couette flow device can cease to be concentric and may evolve to helical, generating erroneous measurements for viscosity as an apparent thickening shear regime emerges (Taylor, 1923). Such transition is characterized by a critical Reynolds number, considering valid measurements in which the Taylor Reynolds number (Re_T) is greater than or equal to their Couette Reynolds number (Re_C):

$$Re_T = 41.3\frac{R_o}{R_o - R_i} \geqslant \frac{\Omega R_i(R_o - R_i)\rho}{\mu} = Re_C. \tag{22}$$

Here, R_i and R_o the internal (and rotating) and external cylinder radii, respectively. We can re-write the condition expressed in the inequality in terms of geometric and rheological parameters of the measuring device and the suspension, $\dot{\gamma}_{\text{rep}}$ and δ (Eqs. (7), (8)), resulting on (23):

$$\frac{\rho\dot{\gamma}_{\text{rep}}}{\mu}\frac{(\delta^2-1)(\delta-1)^2R_i^2}{(1+\delta^2)41.3} \leqslant 1, \tag{23}$$

which we may re-order to identify three non-dimensional contributions to the stability accounting for i) particle hydrodynamics near the wall, ii) length ratio of the inner cylinder and the particles and iii) measuring gap:

$$Re_{p,w}\left(\frac{R_i}{a}\right)f(\delta) \leqslant 1, \tag{24}$$

with a a representative particle radius and f a function obtained from (23), accounting for the geometry of the Couette apparatus. A rough calculation using the parameters of our Couette apparatus and the suspensions here studied showed that $\dot{\gamma} = 400\text{s}^{-1}$ could be safely used as an upper bound in the rheology assessment protocol.

4.2.5. Other sources

Among the other sources of error that we can consider, we may find:

Wall-slip. It has been shown that the slip layer ϵ is a function of the roughness of the rheometry apparatus. In particular, if its roughness is within the same order of the characteristic dimension of the particles, ϵ becomes negligible (Isa et al., 2007). It has also been observed that ϵ might be concentration-dependent, being lower at higher concentrations, but without implying that its effect is less (Barnes, 1995).

Particle settling. From an analysis of the different dimensional groups that control the flow in a Couette cell, Ihle et al. (2013) suggest that shear-induced migration of particles had a greater influence on variations of the measurements for shear rate times on the order of one minute. Therefore, sedimentation is rather a second-order effect compared with wall-slip and other hydrodynamic effects.

Particle migration. These effects are a result of normal stresses between particles (Morris and Boulay, 1999) and are most relevant when the flow passage is wide (although neither solving for normal stresses nor using a Couette geometry, Allende and Kalyon, 2000, make a point in this regard with a set of numerical simulations in Poiseuille flows).

Structural equilibrium. Hyper-concentrated mineral pulps may have an important thixotropic component, which can be explained from the structures that arise from the interaction of individual particles, especially when their clay content is high. Such structures may aggregate or be destroyed at a rate that depends on $\dot{\gamma}$, the solid phase mineralogy, and time. After a long enough time (t_1), the rate of structural change will approach zero and a dynamic equilibrium would be reached. Then, the suspension may be understood as an equivalent suspension of Structural Units (SUs), whose size determines its rheological behavior (Quemada, 1998).

4.3. Rheological data analysis

4.3.1. Variability estimation: steady state measurements

Following the experimental protocol presented in Section 3.3.2, data points for the construction of the $(\dot{\gamma}, \tau)$ profile are obtained from separate tests where $\dot{\gamma}$ was held constant $\dot{\gamma} = \dot{\gamma}_0$ over time t_{exp}, recording n data points. The value for τ would correspond to the average of the τ_{exp} measurements recorded after $t = t_1$, where the suspension is supposed to reach the structural equilibrium described in Section 4.2.5. The t_1 value can be estimated as the first time $t_{\text{exp}}(k^*)$ where the expression (25), accounting for the absolute deviation from the mean in a mobile time frame, is held for an arbitrary user-customizable tolerance $\Delta\widetilde{\tau}$.

$$\sum_{k=k^*}^{n}\left|\tau(k) - \sum_{k'=k^*}^{n}\frac{\tau(k')}{n-k^*+1}\right| \leqslant \Delta\widetilde{\tau}(n-k^*+1) \tag{25}$$

4.3.2. Variability estimation from triplicate shear stress measurements

A typical laboratory procedure to evaluate variability from a rheological measurement is to perform a limited set of measurements and fit each set to the desired rheological model (it is most common to perform measurements in triplicate). If the variability associated to the corresponding fit parameters (*e.g.*, Bingham viscosity, yield stress, flow index, etc.) is high, the flow curve that drifts the most from the average would be probably discarded and the test repeated. If they are all similar, then it is common to consider the average and the standard deviation of the fit parameters multiplied by a penalizing factor to fix a confidence interval (*e.g.*, in this context, Ndlovu et al., 2014) or, more conservative, taking the extreme values of the set of measurements (Reyes et al., 2019). Here, we assess the impact of variability at the shear stress level. To estimate the average and standard deviation, the following relations are used:

$$\bar{\tau} = \frac{1}{n}\sum_{i=1}^{n}\tau_i, \tag{26}$$

$$s^2 = \frac{1}{n-1}\sum_{i=1}^{n}(\bar{\tau} - \tau_i)^2, \tag{27}$$

The sample mean $\bar{\tau}$ follows a t-Student distribution with $n-1$ degrees of freedom, unknown mean μ and standard deviation $\frac{s}{\sqrt{n}}$. For a test repeated n times, the margin of error derived from an $(1-\alpha)$-confidence interval, understood as half its range, is given by (28),

$$m = \frac{t^*}{\sqrt{n}}s, \tag{28}$$

where t^* is the upper $(1-\alpha)/2$ critical value for the $t(n-1)$ distribution. Fig. 5 presents a graphical description of the application of the method described above to the rheological characterization of a mineral suspension, highlighting that the real uncertainty band associated with the triplicate measurement of a variable is higher than the predictions of the other approaches mentioned on this section. In particular, when $n = 3$ and $\alpha = 0.05$ (95% confidence intervals), t^* decreases significantly. This is shown in Table 2, which also shows that under the standard approach, the impact of increasing the number of samples from 3 decreases rapidly.

4.4. Inverse problem for the rheological characterization

4.4.1. Classical formulation

During the rheological test described in Section 3.3.2, experimental

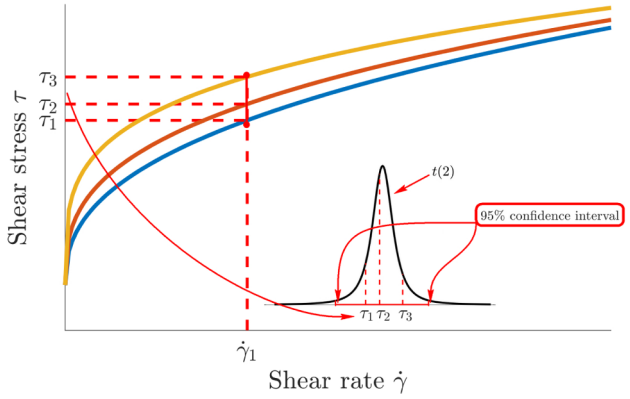

Fig. 5. Variability assessment using triplicate measurements.

Table 2
Multiplicative factors for the 95% confidence intervals of a *t*-Student (two-sided critical region) distribution.

n	Multiplicative Factor t^*
2	12.71
3	4.30
4	3.18
5	2.78
∞	1.96

shear stress τ measurements were performed for different shear rates $\dot{\gamma}$, which were held constant over a fixed time, generating various different τ_{exp} and $\dot{\gamma}_{exp}$ vectors. To interpolate, different rheological models may be used. These models involve a number of parameters, which we will call θ. A common way to formulate and solve a parametric fit problem is by minimizing a cost function J, which accounts for the difference between the modeled curve and the experimental measurements. Generally, and for the sake of simplicity, this function is proportional to the well-known mean square error (denoted herein as MSE), and the problem stated as a least-squares estimation (Marquardt, 1963). By providing physical thresholds for every parameter (the components of vector θ) we may build a provisional feasible set F_0, and, if further information regarding estimates of the parameters is available, θ^*, it is possible to add a regularization contribution J^*_{reg} to the cost function, to penalize parametric values that drift considerably from the reference:

$$J_{reg} = \|\theta - \theta^*\|. \tag{29}$$

Thus, the optimization problem P for curve-fitting, hence parameter estimation, is set as follows:

$$P = \min_{\theta \in F_0} \frac{1}{n+1} \sum_{i=1}^{n} (\tau_{exp}(i) - \tau_{mod}(\dot{\gamma}_{exp,i}))^2 + \epsilon\|\theta - \theta^*\|, \tag{30}$$

whose solution is the set of parameters that best describes the rheological properties of the suspension.

4.4.2. Monte Carlo simulation of rheological parameter variability

Based on the experimental values τ_{exp}, $\dot{\gamma}_{exp}$ and their 95% confidence intervals ($2m_i$, as defined in Eq. (28)), a number N of τ_{sim} and $\dot{\gamma}_{sim}$ random vectors are built, aiming to simulate the curves that may exist within the reported experimental variability frame. Without loss of generality, the aforementioned vectors are represented by (31):

$$\tau_{sim} = \tau_{exp} + m_\tau(2\mathscr{U} - 1), \tag{31}$$

where $\mathscr{U}$ is a random variable with uniform distribution in the [0, 1] interval, and m_τ the error margin (Eq. (28)) of τ. Afterward, each simulated curve ($\dot{\gamma}_{sim}$, τ_{sim}) is individually fitted, and collecting the individual fitted parameters, statistic distributions are obtained. This is depicted schematically in Fig. 6. The reported values are statistically calculated from such distributions, based on their nature (Gaussian, log-normal, gamma, beta, among others) and the author's criteria. For example, if we are trying to obtain the Bingham parameters of a suspension using the rheograms obtained with the protocol described in Section 3.3.2, they are given by Eqs. (32)–(34).

$$[\tau_0^i, \mu_B^i] = \underset{\theta \in F}{\operatorname{argmin}} \left\{ \frac{1}{n+1} \sum_{k=1}^{n} (\tau_{sim}{}^i(k) - \tau_{mod}(\dot{\gamma}^i_{sim,k}))^2 + \epsilon|\theta_i - \theta_i^*| \right\}, \tag{32}$$

$$\tau_0 = \mathbb{E}(\tau_0) \pm \sqrt{\mathrm{Var}(\tau_0)}, \tag{33}$$

$$\mu_B = \mathbb{E}(\mu_B) \pm \sqrt{\mathrm{Var}(\mu_B)}, \tag{34}$$

where the subscripts mod and sim represent the model's solution and the Monte Carlo simulated profiles, respectively.

4.4.3. Application to rheological model fitting

Concentration-dependent rheology models, such as the Heymann model for τ_0, have a higher complexity as significant variable uncertainty is present in both axes. Assuming that the curve-fitting for each rheogram is achieved by our method, the variability in τ_0 is known. Variability in ϕ can be estimated by (12) and experimental data. Thus, simulated variables are represented by (35) and (36).

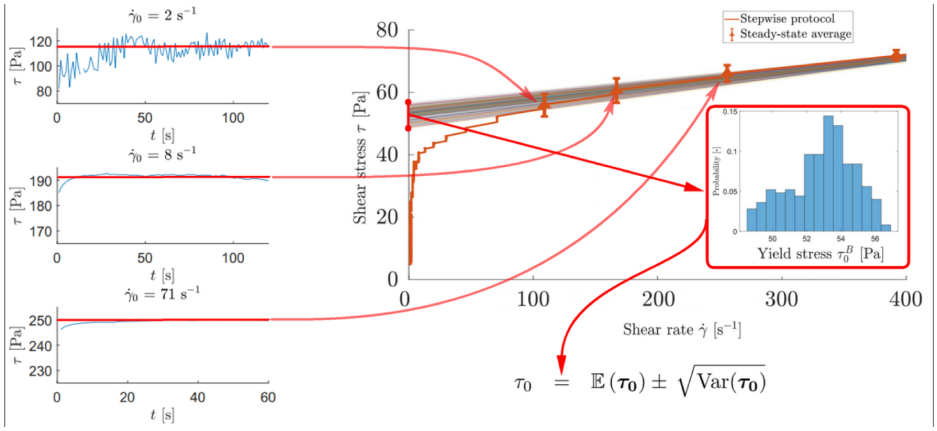

Fig. 6. Inverse problem-solving strategy. The cost function to minimize at the curve-fitting stage is, in spirit, the same, but varies the number N of curves to be fitted. Within the experimental uncertainty, a set of potential curves that could occur given the uncertainty of particular values of $\dot{\gamma}$ are simulated and individually fitted. The reported parameters are statistically obtained from the resulting distributions.

$$\tau_0^{\text{sim}} = \mathbb{E}(\tau_0) + \sqrt{\text{Var}(\tau_0)}\,(2\mathscr{U} - 1), \tag{35}$$

$$\phi^{\text{sim}} = \bar{\phi} + \sigma_\phi(2\mathscr{U}' - 1) \tag{36}$$

The inverse problem can be solved in separate curve-fitting stages, or fitting all the curves together by modifying the cost function and the parametric domain depending on the dimension of the problem and the objective of the study. In the case study considered below we have followed the former strategy.

5. Results and discussion

5.1. Case study: Interplay between rheological models and experimental data processing protocols

Using the statistical approach described above, we assess the applicability of the Herschel-Bulkley and Bingham models under different measuring protocols and curve-fitting strategies. To do so, we simulated two different materials following the aforementioned models, keeping the values for $K = 0.375\text{Pa s}^n$, $n = 0.7$ and $\mu_B = 0.5\text{Pa s}$ fixed, with τ_0 ranging from 10 to 500 Pa. An experimental noise was included to account for potential inappropriate experimental conditions or measuring protocols. To this purpose, we assumed that triplicate experimental measurements involved a relative error of $s = 1\%$, which resulted in a variability bound of $\pm\,5\%$ (using Eq. (28) for a 95% confidence interval). In all cases, measurements have been made at shear rates well below the onset of the Taylor-Couette instability, at shear rate intervals with the shape $I_{\dot\gamma} = [\dot\gamma_1, 400]\,\text{s}^{-1}$, where $\dot\gamma_1 \in \{0.01;0.1;1;10;100\}$. The curve-fitting procedure considered a logarithmic 15-point partition of $I_{\dot\gamma}$, and $N = 250$ simulated curves were employed for the Monte Carlo-inspired assessment of the parameters. Further discussions regarding the number of points for the curve-fitting procedure and the number of Monte Carlo simulated profiles are presented in Section 5.3.

The coefficient of variation of the τ_0^{HB} distributions (defined by Eq. (9)) was obtained for different curve-fitting protocols and presented in Fig. 7. When $\dot\gamma_1$ approaches to 0s^{-1}, the parameter distributions presented less variability and, consistently with Eq. (33) (applied to the corresponding model), their expected values provided better estimators of the suspension's rheological properties. Regarding the Bingham model (Fig. 7a), CV trends seem to have high variability in τ_0^{B} at low τ_0^{control} values, resulting from (9) when $\mathbb{E}(\tau_0) \to 0$. This effect is enhanced increasing $\dot\gamma_1$ and is explained by the proportional nature of the induced error s and the extrapolative nature of the method.

Different is the case for the HB materials (Fig. 7b), as an increasing trend in CV is observed for all protocols when the reference τ_0^{control} increases. The preceding observation seems not only to be a result of the extrapolative nature of the method but of the mathematical properties of the HB model. A closer look at the nature of the variability in τ_0^{HB} is presented in Fig. 8. It can be seen that the prediction of τ_0^{HB} systematically underestimates its real value, especially for protocols with $\dot\gamma_1 \geqslant 1$, as the width of the uncertainty bands increases with the control τ_0^{control}. The additional degree of freedom that a third parameter (n) gives to the curve shape in the HB model and the potential for inappropriate curve-fitting protocols for intercept determination (Fig. 7b), generate higher variability in the results. Conversely, protocols with high resolution at low shear rates result in distributions with less variability, as Fig. 8 shows. Although the uncertainty bands remain considerable, the coefficient of variation and relative error decrease, as shown in Table 3. The foregoing highlights the applicability of our method to retrieve the rheological parameters that best describe the suspension, even when the experimental variability is high.

An analysis of the effect of experimental error on the variability of τ_0^{HB} for a typical curve-fitting protocol is presented in Fig. 9. Even considering a variability frame of $m = 1\%$, obtained by applying Eq. (28) to a triplicate test with experimental error $s = 0.4\%$, the variability in τ_0^{HB} remains considerable, especially when evaluating suspensions with high yield stresses.

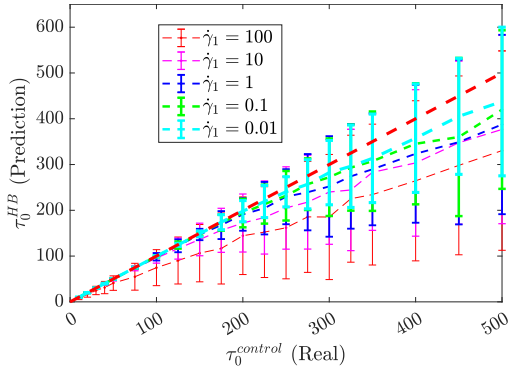

Fig. 8. Variability in the prediction of τ_0^{HB}, for different curve-fitting protocols. The expected values of the τ_0^{HB} distributions (dashed lines) seem to be better estimators of τ_0 when the curve-fitting interval starts closer to zero.

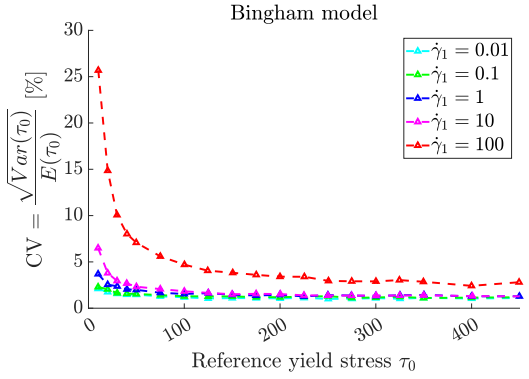

(a) A greater variability in τ_0^{B} may only be observed at low shear rates, due to the singularity CV in $\mathbb{E}(\tau_0) = 0$. As the coefficient of variation approaches to a horizontal asymptotic line, the induced proportional noise seems to be the reason of the observed variability.

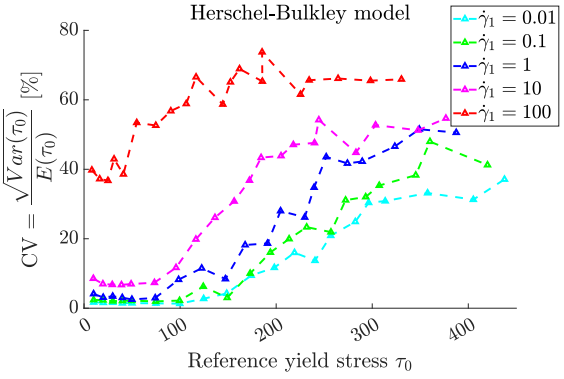

(b) Higher variability in τ_0^{HB} is observed when the fitting interval $I_{\dot\gamma}$ starts at a higher value of $\dot\gamma$. As the variability in τ_0^{HB} increases with τ_0^{control}, the non-linear characteristic of the HB model (given by the flow index $n < 1$) propagates to the induced noise.

Fig. 7. Effect of the shear rate interval chosen to fit the selected rheological model on the quality of the outcome.

Table 3
Dispersion metrics of the HB and Bingham yield stress for different curve-fitting intervals, with $\tau_0^{control} = 100$ Pa.

curve-fitting interval $I_{\dot\gamma}$ [s^{-1}]	Herschel-Bulkley		Bingham	
	CV [%]	e_{rel} [%]	CV [%]	e_{rel} [%]
0.01–400	1.31	0.32	1.18	0.08
0.1–400	2.19	0.56	1.29	0.02
1–400	8.24	1.56	1.54	0.01
10–400	11.68	4.24	1.83	0.03
100–400	52.61	25.3	4.70	0.19

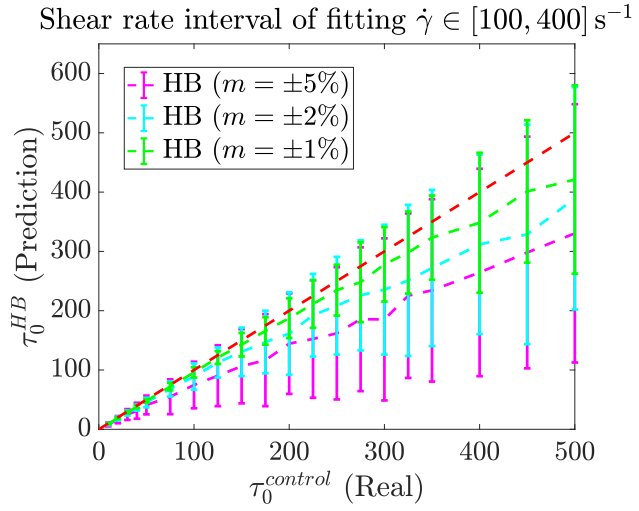

Fig. 9. Effect of the experimental variability on the rheological parameter determination. Even assuming that the experimental measurements are confined in a $m = 1\%$ variability frame, if the curve-fitting procedure is not appropriate, it is not possible to obtain precise Herschel-Bulkley parameters.

5.2. Case study: Risks behind the standard rheological data analysis procedure

Typically, parameters and errors associated with the rheological characterization of mineral pulps are reported as the simple average and the standard deviation of a triplicate individual test fit. Note that the *triplicate method* (TM) only refers to the post-processing of the parameters resulting from a curve-fitting procedure. This method consists of three steps:

- Triplicate rheological test.
- Individual curve-fitting of the experimental profiles obtained in Step 1 to obtain rheological parameters.
- Reporting respectively parameters' values and variability as the mean and standard deviation, range (or weighting of such dispersion metrics) of the results of Step 2.

The use of the TM has limitations due to:

1. There are non-linearities in the pulp's rheological behavior and the models used to represent it. Therefore, the curve resulting from the average of parameters might be biased when compared to the curves obtained by the individual parameters.
2. The nature of the error distribution is unknown. Hence, the average of triplicate parameters might not be a good estimator of their real value, nor the standard deviation of their true variability.

To assess how much variability lies on the TM, we performed the following experiment. First, considering the same simulated materials

Table 4
Evaluation of the TM for the Herschel-Bulkley model. Several trios of simulated curves were selected from the N-Monte Carlo pool, having 2573000 possible combinations of experimental profiles that are equally probable. Out of the different possibilities, the best and worst scenarios, regarding the width of the 95% confidence interval, are highlighted. The high variability in the reported variability (range of the confidence intervals) suggests that the TM should not be used to assess this concept.

Reference $\tau_0^{control}$ [Pa]	Least variance triplicate scenario		Most variance triplicate scenario		Average triplicate scenario		Variability of the triplicate variability
	τ_0^{HB}	$\frac{t^*}{\sqrt{3}}s$ (Eq. (28))	τ_0^{HB}	$\frac{t^*}{\sqrt{3}}s$ (Eq. (28))	$\langle\tau_0^{HB}\rangle$	$\sigma_{\tau_0^{HB}}$	$\sqrt{\mathrm{Var}(s_{\tau_0^{HB}})}$
10	9.7	0.001	9.7	4.5	9.9	0.2	0.2
20	19.8	0.000	20.1	6.7	19.9	0.3	0.3
30	29.0	0.002	30.2	9.0	29.9	0.4	0.3
40	39.4	0.005	40.0	12.5	39.9	0.6	0.5
50	50.0	0.002	50.1	14.7	49.8	0.7	0.6
75	75.0	0.006	75.2	22.2	74.6	1.0	0.9
100	100.5	0.004	74.5	190.9	98.4	3.6	5.4
125	125.0	0.010	86.9	280.1	122.5	7.1	11.1
150	150.5	0.016	104.1	335.7	146.7	7.1	10.8
175	176.5	0.007	61.4	394.6	168.5	15.4	23.9
200	198.6	0.005	70.0	451.5	187.6	23.8	36.0
225	223.5	0.003	78.8	507.9	210.3	27.9	42.0
250	251.9	0.019	87.5	564.4	228.9	35.0	50.8

discussed in Section 5.1, N curves were randomly selected from the variability frame of ± 5%, and fitted in the $I_{\dot\gamma} = [1, 400]s^{-1}$ interval considering 15 data points for that procedure. Then, we obtain all the possible subsets of 3 curves from the N-pool and calculate the sample average and standard deviation of their parameters. As we used $N = 250$ for the Monte Carlo simulations, the different possibilities for the triplicate selection are exactly $\binom{250}{3} = 2573000$ curves. Table 4 shows the results of this analysis for τ_0^{HB}. The least variance triplicate scenario (out of the 2573000 possibilities) and average triplicate scenario were studied, highlighting how dramatically a favorable scenario could mislead the conclusions on the rheological behavior of the sample (see the 6th column in Table 4). Moreover, the variability of the reported triplicate variability (understood as a distribution s) was in most of the cases higher than the N–population's standard deviation. As the TM-reported variability is unreliable, we suggest not to consider it as an estimator of the real variability of the parameter.

5.3. Case study: On the stability of our method

To test how stable our approach and assumptions are, we performed two numerical experiments. A first one to determine how heavily the number of points (resolution) considered for the curve-fitting procedure impacted on the variability of the inferred parameters. The second, to obtain the optimal number of Monte Carlo simulations to make the variability of the measurements converge to its real value.

5.3.1. Number of data points considered for curve-fitting

The number of data points considered for curve-fitting corresponds to the resolution of the curve-fitting interval $I_{\dot\gamma}$ and is part of the design of the measurement protocol, given the particularities of the tested material and the limitations of the measuring instrument. We tested different curve-fitting intervals with the form $I_{\dot\gamma} = [\dot\gamma_1, 400]$. Fig. 10 shows the trends of the dispersion of the obtained distributions when the number of data points for the curve-fitting procedure varied, considering two curve-fitting intervals. When $\dot\gamma_1 = 1\ s^{-1}$ (Fig. 10a), the variability of the values of τ_0^{HB} decreases as the resolution of the curve-fitting interval increases, suggesting that having more measurements

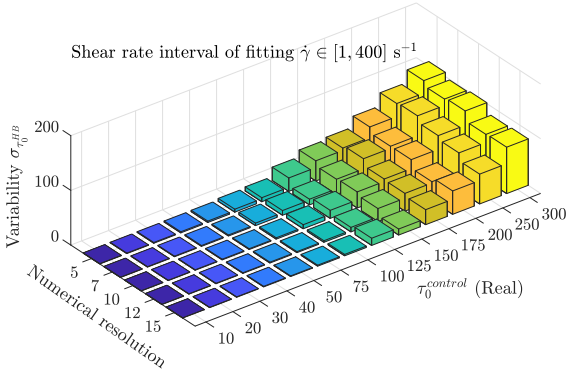

(a) When the curve-fitting interval allows a close calibration of the intercept with the $y-$axis (τ_0^{HB}), improving the resolution of the experimental plan reduces the variability of the inferred parameters.

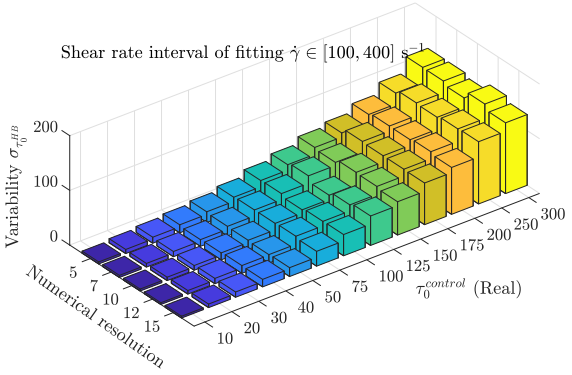

(b) When the curve-fitting interval does not allow a close calibration of the intercept with the $y-$axis (τ_0^{HB}), improving the resolution of the experimental plan does not have a positive impact on the variability of the inferred parameters.

Fig. 10. Effect of the resolution of the curve-fitting procedure on the variance of the inferred parameters.

would positively impact the quality of the inferred parameters. When $\dot{\gamma}_1 = 100$ s^{-1} (Fig. 10b), the variability of the values of τ_0^{HB} does not show any improvement when increasing the resolution of the curve-fitting interval. As stated above, dense experimental planning, which in this context refers to a plan considering several different shear rates, should only be carried out when the resolution of the equipment allows the implementation of wide curve-fitting intervals.

Our results suggest that the lower bound of the curve-fitting interval should always be equal to the lower limit of the measuring equipment, $\dot{\gamma}_1$. The density of experiments performed between $\dot{\gamma}_1$ and the upper bound of the planned shear rate interval seems to be a function of such value and would help to reduce the variance in the inferred parameters only if $\dot{\gamma}_1$ is close enough to 0.

5.3.2. Number of Monte Carlo simulations

The number of curves to simulate within the experimental variability described in Section 4.4.2, which at first sight might look an arbitrary election, is the result of a delicate trade-off between accuracy and computational cost. To obtain the optimal number N of curves, we performed an analysis of convergence of the variability of τ_0^{HB} considering a different number of curves to fit over the same intervals considered in Section 5.3.1, with a resolution of 15 experimental points. As N increases, the reported variability quickly converges to the steady-state for both considered curve-fitting intervals (see Fig. 11). The convergence of the first interval seems to be more erratic than the second. Nevertheless, the amplitude of such deviations is much lower, as the curve-fitting interval is wide.

5.4. Case study: Effect of NaCl concentration on tailing rheology

In order to study the effect of high concentrations of NaCl on the rheology of synthetic tailings —blends of quartz and kaolinite/bentonite—, we followed the steps for the identification and quantification of error proposed in Section 4.2. Given that bentonite is classified as a swelling clay, special attention was paid to the concentration of the suspension ϕ. Using as a pre-shear the hysteresis loop discussed in Section 3.3.2 and the collection of step-wise tests to assess the temporal evolution of τ at a constant shear rate, presented in Table A.5, we applied our methodology to obtain the Bingham yield stress τ_0. Using our method to estimate the variability of τ_0^B, and Eq. (12) for uncertainties in ϕ, it was possible to obtain both the vertical and horizontal components of the errorbars on a (ϕ, τ_0^B) plot. The uncertainty intervals mentioned above are a crucial input to differentiate the real trends from the variability-induced interpretations.

The Heymann model (Heymann et al., 2002) provides a qualitative picture of the dependence of the yield stress on the concentration in mineral suspensions *via* crowding and is proportional to a structural parameter (τ^*) which, in light of the relative positions of the curves of the KK and MK cases in Fig. 12, suggests a decreasing trend with salt concentration, as seen by the vertical offset of curves. This has been also

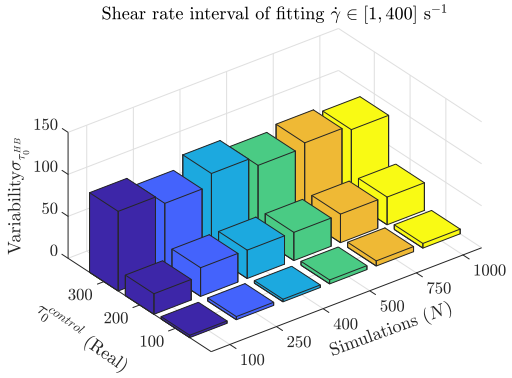

(a) When the curve-fitting interval allows a close calibration of the intercept with the $y-$axis (τ_0^{HB}), the convergence of Monte Carlo simulations seems to be slower than in 11b. Nevertheless, the steady state value is much lower, suggesting that fluctuations around the invariant value might be proportional.

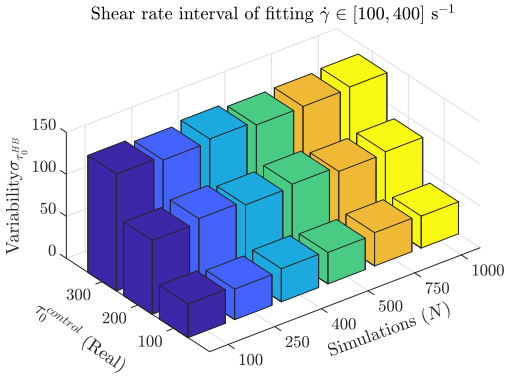

(b) When the curve-fitting interval does not allow a close calibration of the intercept with the $y-$axis (τ_0^{HB}), the variability of the Monte Carlo simulations reaches quickly their steady-state value.

Fig. 11. Convergence of the Monte Carlo simulations.

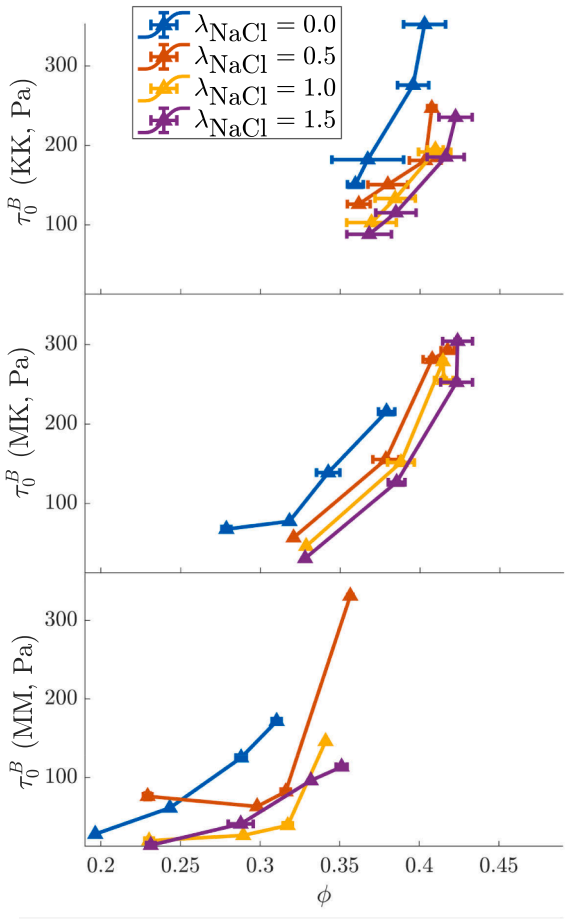

Fig. 12. Effect of the salinity of the medium on the rheology (Bingham yield stress) of clay suspensions. As discussed in the previous sections, the Bingham yield stress τ_0^B presents little variability, and the uncertainty in the solid concentration is the main contribution to variability. Nevertheless, a clear trend is observable for all the synthetic tailings, as higher NaCl concentrations seem to produce lower yield stresses in the suspensions.

found with direct measurements of the yield stress using a vane rheometer (Jeldres et al., 2017). The increase on the yield stress with the concentration is considerably stronger in the MM case (bottom panel of Fig. 12). In other words, the ϕ-τ_0^B curves in the MM case are offset to the left compared to the KK and MK curves. Common structural interpretations based on SEM images of pure clays (*i.e.* structural re-organization from edge-face to edge-face) can be referred to partially explain the interplay between clays and mineral polymineralic suspensions. This includes the decreasing behavior of yield stress with the salt content for salt concentrations below *ca.* 10^{-2} M (Van Olphen, 1955), a further increase for concentrations up to *ca.* 0.1 M (Rand et al., 1980), and an influence on double-layer compression at even higher salt contents. A specific study focused on the effect of clay/mineral blends has been recently reported by Merrill et al. (2017), who found synergistic effects from blending bentonite from different sources (and thus differing accessory mineral content and fine particle size distribution) and conjectured that besides the aforementioned edge-face charge heterogeneity effect, there are non-DLVO effects derived from competitive ion adsorption. This somewhat coincides with the fact that the MM sample has the greatest cation exchange capacity among the three cases studied herein, and brings the attention to the conceptually more complex scenario that involves the MM case.

The foregoing confirms the experimental observations of this study for the various synthetic tailings evaluated, presented in Fig. 12, which show a predominant decreasing trend of the ϕ-τ_0^B curves over the range of salinity studied, saturating to higher salinity at different rates that seem to depend on the mineralogy of the suspension. From a process control perspective, the impact of sample characteristics on their variability is somewhat hidden by the present lack of available models on the impact of the mineralogy in the MM case. In the particular process of clay-laden long distance tailing transport, it would be beneficial to bound input variability through knowing which, and in what amount, auxiliary clays (potentially under the presence of salt) could be added to reduce both water and specific energy consumption. This is essentially a water resource, rheological and economic problem. Such knowledge would not only serve to the present approach, based on fitting rheograms obtained from Taylor-Couette cells, but also to related inverse problems on the rheological parameters, both associated to generic inverse modelling as presented in (1) and others based on Poiseuille flow rheometry (Barnes et al., 1989; Ihle and Tamburrino, 2012a), for online rheology measurement purposes.

6. Conclusions

We have developed a novel statistically-based methodology to assess the reliability of model-derived rheological parameters, which can be easily extended to other control parameters commonly used in mineral processing. First, we describe some of the error sources that may appear in the rheological characterization of concentrated mineral suspensions, addressing the limitations of the different protocols and providing mathematical expressions for proper error propagation. Then, we statistically calculate the variability frame of the experimental measurements, understood as the 95% confidence intervals. Using a Monte Carlo-inspired approach, we simulate all the experimental curves that may exist within such variability frame. We individually obtain the parameters of selected rheological models following a customizable curve-fitting protocol, resulting in distributions of rheological parameters. Finally, from such distributions, we statistically obtain the suspension's rheological parameters and estimate their variability, with a computational approach which is modest in computer resource demands. Even though it is possible to accurately characterize the rheological behavior of a suspension through multiple steady-state tests (measuring τ over time, at a given $\dot{\gamma}$), we propose the present method as a way to estimate such behavior in shorter times, thus improving variability assessment.

We used our method to evaluate the impact that the data processing protocol has on the variability of the resulting rheological parameters and compared our results with those obtained using the triplicate method. The Herschel-Bulkley model showed to be very sensitive to the curve-fitting interval, especially when such interval was not close to $\dot{\gamma} = 0$, being unsuitable for predicting high yield stresses. The present approach suggests to complement rheology measurements with additional data. Doing so, we would have a regularization point for the curve-fitting algorithm within a shear rate zone without access to data points (*e.g.* due to wall slip) and a threshold for the yield stress value, thus reducing its variability while keeping flow curve parametric fitting rationale. Studying the effect of experimental noise on the variability of the model-derived parameters, it was possible to observe a strong relationship between experimental accuracy and parametric precision. Furthermore, when combining the effects of experimental resolution, data processing protocol, and the complexity of the applicable mathematical model, it is possible to explore the boundaries of the accuracy that could be achieved (with given resources) while calculating model-derived parameters.

We have applied our methodology in a case study, obtaining useful insights regarding the effect that high NaCl concentrations might have on copper sulfide tailings bearing a high clay content. The present work finally stresses the key role that addressing variability in experimentally determined parameters has for proper operational forecasting and control.

CRediT authorship contribution statement

Sebastián Contreras: Conceptualization, Methodology, Software, Formal analysis, Investigation, Data curation, Writing - original draft, Visualization. **Claudia Castillo:** Conceptualization, Methodology, Investigation, Writing - review & editing. **Álvaro Olivera-Nappa:** Methodology, Writing - review & editing. **Brian Townley:** Validation, Writing - review & editing. **Christian F. Ihle:** Conceptualization, Methodology, Investigation, Resources, Validation, Writing - original draft, Funding acquisition.

Declaration of Competing Interest

The authors declare that they have no known competing financial interests or personal relationships that could have appeared to influence the work reported in this paper.

Acknowledgements

The authors gratefully acknowledge support from the Department of Mining Engineering of University of Chile, the Centre for Biotechnology and Bioengineering - CeBiB (PIA project FB0001, Conicyt, Chile), the Chilean National Agency for Research and Development through Fondecyt Project 1160971 and PIA Grant AFB180004, Project INNOVA CORFO Project CSIRO Chile 10CEII- 9007. The authors would also like to thank Dr. Ricardo Jeldres for helpful discussions, and Gabriel Mendez for undertaking the rheological measurements presented in the Case of Study.

Appendix A. Flow curve measurement sequence

The flow curve measurement sequence is detailed in Table A.5.

Table A.5
Flow curve measurement sequence.

Shear rate $\dot{\gamma}$ [s^{-1}]	Time [s]
1 → 400	120
400	30
400 → 1	120
1.0	120
1.5	120
2.3	120
3.6	120
5.5	120
8.4	120
12.9	60
19.8	60
30.3	60
46.4	60
71.1	60
109.0	30
166.9	30
255.7	30
391.7	30
600.0	30

Appendix B. Error propagation for solids concentration ϕ

B.1. Analytical error propagation

Table B.6 shows the analytical components of $\nabla\phi$ and H_ϕ used in the error propagation analysis.

Table B.6
Analytical components of $\nabla\phi$ and H_ϕ for error propagation analysis.

Derivative		Functional expression
$\frac{\partial\phi}{\partial\rho_s}$	=	$-\phi^2\left(\frac{1-C_p}{\rho_l C_p}\right)$
$\frac{\partial\phi}{\partial C_p}$	=	$\left(\frac{\phi}{C_p}\right)^2\frac{\rho_s}{\rho_l}$
$\frac{\partial^2\phi}{\partial\rho_s^2}$	=	$2\phi^3\left(\frac{1-C_p}{\rho_l C_p}\right)^2$
$\frac{\partial^2\phi}{\partial\rho_s\partial C_p}$	=	$\left(\frac{\phi}{C_p}\right)^2\frac{1}{\rho_l}\left(1-\frac{2\phi(1-C_p)}{C_p}\frac{\rho_s}{\rho_l}\right)$
$\frac{\partial^2\phi}{\partial C_p^2}$	=	$\frac{2\phi^2}{C_p^3}\left(\frac{\rho_s}{\rho_l}\right)\left(\frac{\phi}{C_p}\frac{\rho_s}{\rho_l}-1\right)$

B.2. Sensitivity analysis

To assess the parameters' contribution to the variability in the solids concentration, ϕ, a sensitivity analysis at medium and high values of the relative error in terms of such variable has been carried out. As shown in Fig. B.13, the impact of small variations in the solid density ρ_s seems not to be relevant, especially at high values of ϕ. On the other hand, small variations in C_p may have a considerable effect on reported values of ϕ, especially when ϕ is close to the maximum packing fraction of the suspension, ϕ_m.

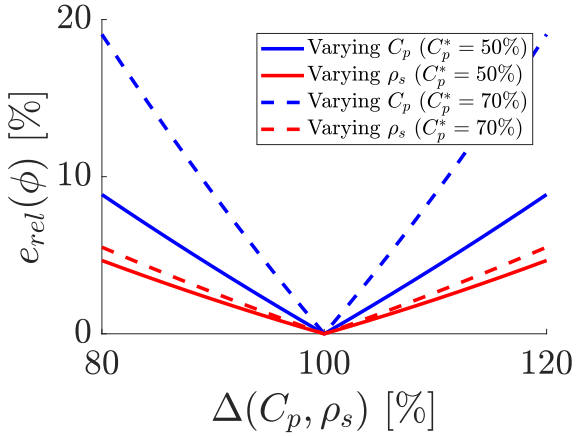

Fig. B.13. Sensitivity analysis of ϕ before small perturbations in ρ_s^* and C_p^* at $C_p^* = 50\%$ (a), and $C_p^* = 70\%$ (b), both considering $\rho_s^* = 2.7\text{t/m}^3$. Greater slopes mean greater sensitivity to changes in the corresponding parameter since small variations would imply significant changes in the reported error.

References

Abichequer, L.A., Costa, J., Pasti, H.A., Koppe, J.C., 2011. Design of blending piles by geostatistically simulated models-A real case reconciliation. Int. J. Miner. Process. 99, 21–26.

Alejo, B., Barrientos, A., 2009. Model for yield stress of quartz pulps and copper tailings. Int. J. Miner. Process. 93, 213–219.

Allende, M., Kalyon, D.M., 2000. Assessment of particle-migration effects in pressure-driven viscometric flows. J. Rheol. 44, 79.

Astarita, G., 1990. Letter to the Editor: The engineering reality of the yield stress. J. Rheol. 34, 275–277.

Avramidis, K.S., Turian, R.M., 1991. Yield stress of laterite suspensions. J. Colloid Interface Sci. 143, 54–68.

Barnes, H., Walters, K., 1985. The yield stress myth? Rheologica Acta 24, 323–326.

Barnes, H.A., 1995. A review of the slip (wall depletion) of polymer solutions, emulsions and particle suspensions in viscometers: its cause, character, and cure. J. Nonnewton. Fluid Mech. 56, 221–251.

Barnes, H.A., Hutton, J.F., Walters, K., 1989. An Introduction to Rheology, vol. 3 Elsevier Science.

Basnayaka, L., Subasinghe, N., Albijanic, B., 2017. Influence of clays on the slurry rheology and flotation of a pyritic gold ore. Appl. Clay Sci. 136, 230–238.

Boger, D.V., 2009. Rheology and the resource industries. Chem. Eng. Sci. 64, 4525–4536.

Boger, D.V., 2013. Rheology of slurries and environmental impacts in the mining industry. Ann. Rev. Chem. Biomol. Eng. 4, 239–257.

Bonn, D., Denn, M.M., 2009. Yield stress fluids slowly yield to analysis. Science 324, 1401–1402.

Calvo, G., Mudd, G., Valero, A., Valero, A., 2016. Decreasing ore grades in global metallic mining: A theoretical issue or a global reality? Resources 5, 36.

Cisternas, L., Moreno, L., 2014. El agua de mar en la minería: Fundamentos y aplicaciones. RIL editores.

Cisternas, L.A., Gálvez, E.D., 2018. The use of seawater in mining. Miner. Process. Extr. Metall. Rev. 39, 18–33.

Connelly, D., 2011. High clay ores–a mineral processing nightmare. Austral. J. Min. 24, 28–29.

Contreras, S., Castillo, C., Ihle, C., Mendez, G., 2019. Characterization of the effect of clay mineralogy and content on the rheological behavior of copper sulfide tailings. In: Proceedings of the 6th International Seminar on Tailings Management, Tailings 2019, pp. 242–250.

Cruz, N., Peng, Y., 2016. Rheology measurements for flotation slurries with high clay contents–a critical review. Miner. Eng. 98, 137–150.

Cullinan, V.J., Grano, S.R., Greet, C.J., Johnson, N.W., Ralston, J., 1999. Investigating fine galena recovery problems in the lead circuit of Mount Isa Mines Lead/Zinc Concentrator part 1: Grinding media effects. Miner. Eng. 12, 147–163.

Gräfe, M., Klauber, C., McFarlane, A.J., Robinson, D.J., 2017. Clays in the Minerals Processing Value Chain. Cambridge University Press.

He, M., Wang, Y., Forssberg, E., 2004. Slurry rheology in wet ultrafine grinding of industrial minerals: a review. Powder Technol. 147, 94–112.

Heath, D., Tadros, T.F., 1983. Influence of pH, electrolyte, and poly (vinyl alcohol) addition on the rheological characteristics of aqueous dispersions of sodium montmorillonite. J. Colloid Interface Sci. 93, 307–319.

Herrera-León, S., Lucay, F.A., Cisternas, L.A., Kraslawski, A., 2019. Applying a multi-objective optimization approach in designing water supply systems for mining industries. The case of Chile. J. Clean. Product. 210, 994–1004.

Heymann, L., Peukert, S., Aksel, N., 2002. On the solid-liquid transition of concentrated suspensions in transient shear flow. Rheologica Acta 41, 307–315.

Ihle, C., 2014. The need to extend the study of greenhouse impacts of mining and mineral processing to hydraulic streams: Long distance pipelines count. J. Clean. Product. 84, 597.

Ihle, C., Tamburrino, A., 2012a. A note on the Buckingham equation. Can. J. Chem. Eng. 90, 944–945.

Ihle, C.F., 2013. A cost perspective for long distance ore pipeline water and energy utilization. Part I: Optimal base values. Int. J. Miner. Process. 122, 1–12.

Ihle, C.F., Kracht, W., 2018. The relevance of water recirculation in large scale mineral processing plants with a remote water supply. J. Clean. Product. 177, 34–51.

Ihle, C.F., Tamburrino, A., 2012b. Uncertainties in key transport variables in homogeneous slurry flows in pipelines. Miner. Eng. 32, 54–59.

Ihle, C.F., Tamburrino, A., Vivero, P., 2013. Effect of sample manipulation on the Couette rheometry of copper concentrates. Powder Technol. 239, 78–85.

Isa, L., Besseling, R., Poon, W.C., 2007. Shear zones and wall slip in the capillary flow of concentrated colloidal suspensions. Phys. Rev. Lett. 98, 198305.

Jeldres, R.I., Piceros, E.C., Leiva, W.H., Toledo, P.G., Herrera, N., 2017. Viscoelasticity and yielding properties of flocculated kaolinite sediments in saline water. Colloids Surf., A 529, 1009–1015.

Knight, A., Sofrà, F., Stickland, A., Scales, P., Lester, D., Buscall, R., 2017. Variability of shear yield stress–measurement and implications for mineral processing. In: Proceedings of the 20th International Seminar on Paste and Thickened Tailings. University of Science and Technology Beijing, pp. 57–65.

Krieger, I.M., 1972. Rheology of Monodisperse Latices. Adv. Colloids Interface Sci. 3, 111–136.

Lin, Y., Cheah, L.K.J., Phan-Thien, N., Khoo, B.C., 2016. Effect of temperature on rheological behavior of kaolinite and bentonite suspensions. Colloids Surf., A 506, 1–5.

Marquardt, D.W., 1963. An algorithm for least-squares estimation of nonlinear parameters. J. Soc. Ind. Appl. Mathe. 11, 431–441.

Mering, J., 1946. On the hydration of montmorillonite. Trans. Faraday Soc. 42, B205–B219.

Merrill, J., Voisin, L., Montenegro, V., Ihle, C.F., McFarlane, A., 2017. Slurry rheology prediction based on hyperspectral characterization models for minerals quantification. Miner. Eng. 109, 126–134.

Montes, C., Cantallopts, J., 2019. Consumo de agua en la minería del cobre al 2018. Technical Report. Comisión chilena del cobre (COCHILCO). Santiago, Chile.

Morris, J.F., Boulay, F., 1999. Curvilinear flows of noncolloidal suspensions: The role of normal stresses. J. Rheol. 43, 1213.

Mpofu, P., Addai-Mensah, J., Ralston, J., 2003. Investigation of the effect of polymer structure type on flocculation, rheology and dewatering behaviour of kaolinite dispersions. Int. J. Miner. Process. 71, 247–268.

Mueller, S., Llewellin, E., Mader, H., 2010. The rheology of suspensions of solid particles. In: Proceedings of the Royal Society of London A: Mathematical, Physical and

Engineering Sciences. The Royal Society, pp. 1201–1228.
Ndlovu, B., Farrokhpay, S., Bradshaw, D., 2013. The effect of phyllosilicate minerals on mineral processing industry. Int. J. Mineral Process. 125, 149–156.
Ndlovu, B., Forbes, E., Farrokhpay, S., Becker, M., Bradshaw, D., Deglon, D., 2014. A preliminary rheological classification of phyllosilicate group minerals. Miner. Eng. 55, 190–200.
Nguyen, Q.D., Akroyd, T., De Kee, D.C., Zhu, L., 2006. Yield stress measurements in suspensions: an inter-laboratory study. Korea-Australia Rheol. J. 18, 15–24.
Nguyen, Q.D., Boger, D.V., 1983. Yield stress measurement for concentrated suspensions. J. Rheol. 27, 321.
Norgate, T., Haque, N., 2010. Energy and greenhouse gas impacts of mining and mineral processing operations. J. Clean. Product. 18, 266–274.
Ovarlez, G., Bertrand, F., Rodts, S., 2006. Local determination of the constitutive law of a dense suspension of noncolloidal particles through magnetic resonance imaging. J. Rheol. 50, 259–292. https://doi.org/10.1122/1.2188528.
Quemada, D., 1977. Rheology of concentrated disperse systems and minimum energy dissipation principle. Rheol. Acta 16, 82–94.
Quemada, D., 1998. Rheological modelling of complex fluids. i. the concept of effective volume fraction revisited. Eur. Phys. J.-Appl. Phys. 1, 119–127.
Rand, B., Pekenć, E., Goodwin, J.W., Smith, R.W., 1980. Investigation into the existence of edge-face coagulated structures in Na-montmorillonite suspensions. J. Chem. Soc., Faraday Trans. 1: Phys. Chem. Condensed Phases 76, 225–235.
Reyes, C., Álvarez, M., Ihle, C.F., Contreras, M., Kracht, W., 2019. The influence of seawater on magnetite tailing rheology. Miner. Eng. 131, 363–369.
Shi, F.N., Napier-Munn, T.J., 1996. A model for slurry rheology. Int. J. Miner. Process. 47, 103–123.
Sofra, F., Boger, D.V., 2011. Rheology for thickened tailings and paste–history, state-of-the-art and future directions. In: Proceedings of Fourteenth International Seminar on Paste and Thickened Tailings (Paste 11), pp. 5–7.
Stickel, J.J., Powell, R.L., 2005. Fluid mechanics and rheology of dense suspensions. Annu. Rev. Fluid Mech. 37, 129–149.
Tangsathitkulchai, C., 2003. The effect of slurry rheology on fine grinding in a laboratory ball mill. Int. J. Miner. Process. 69, 29–47.
Tangsathitkulchai, C., Austin, L.G., 1988. Rheology of concentrated slurries of particles of natural size distribution produced by grinding. Powder Technol. 56, 293–299.
Taylor, G., 1923. Viii. stability of a viscous liquid contained between two rotating cylinders. Philosoph. Trans. Roy. Soc. London A: Mathe., Phys. Eng. Sci. 223, 289–343.
Vallar, S., Houivet, D., El Fallah, J., Kervadec, D., Haussonne, J.M., 1999. Oxide slurries stability and powders dispersion: optimization with zeta potential and rheological measurements. J. Eur. Ceram. Soc. 19, 1017–1021.
Van Olphen, H., 1955. Forces between suspended bentonite particles. Clays Clay Miner. 4, 204–224.
Van Olphen, H., 1964. Internal mutual flocculation in clay suspensions. J. Colloid Sci. 19, 313–322.
Wu, M.Y., Adachi, Y., 2016. Effects of electrolyte concentration and pH on the sedimentation rate of coagulated suspension of sodium montmorillonite. Colloids Surf., A 506, 686–693.
Yu, Y., Ma, L., Cao, M., Liu, Q., 2017. Slime coatings in froth flotation: A review. Miner. Eng. 114, 26–36.